# An Advanced Integrated Visible Light Communication and Localization System

Helin Yang<sup>®</sup>, Senior Member, IEEE, Sheng Zhang, Arokiaswami Alphones<sup>®</sup>, Senior Member, IEEE, Chen Chen<sup>®</sup>, Member, IEEE, Kwok-Yan Lam<sup>®</sup>, Senior Member, IEEE, Zehui Xiong<sup>®</sup>, Senior Member, IEEE, Liang Xiao<sup>®</sup>, Senior Member, IEEE, and Yi Zhang<sup>®</sup>, Member, IEEE

Abstract-Visible light communication (VLC) is an emerging wireless technology to support high transmission rate for indoor devices by using existing lighting infrastructure, and VLC-based indoor localization is capable of providing highaccuracy localization. However, current VLC-based localization systems suffer from several key challenges such as sensitivity to random tilting of the receiver, which limits its full potential in real-world applications. In this paper, we design an integrated visible light communication and localization (VLCL) system to simultaneously support accurate real-time localization and communication services for indoor devices. To achieve this, an advanced differential phase difference of arrival (A-DPDOA) localization design is developed to simplify hardware and improve tracking robustness. In addition, a joint adaptive modulation, subcarrier and power allocation scheme is also proposed, which aims to improve the communication data rate and localization accuracy. Extensive experiments are performed to demonstrate that the proposed integrated VLCL system achieves higher

Manuscript received 25 August 2022; revised 7 April 2023 and 26 June 2023; accepted 23 August 2023. Date of publication 29 August 2023; date of current version 19 December 2023. This work was supported in part by the National Natural Science Foundation of China under Grants No. 62371408, 62301467, 61971366, U21A20444, and 62271091, the Fundamental Research Funds for the Central Universities under Grant No. 20720220080. This research is also supported by the National Research Foundation, Singapore, and Infocomm Media Development Authority under its Future Communications Research and Development Programme. The research is also supported by the SUTD SRG-ISTD-2021-165, the SUTD-ZJU IDEA Grant (SUTD-ZJU (VP) 202102), and the Ministry of Education, Singapore, under its SUTD Kickstarter Initiative (SKI 20210204). An earlier version of this paper was presented in part at the IEEE International Conference on Communications (ICC), Dublin, Ireland, June 2020 [DOI: 10.1109/ICC40277.2020.9149119]. The associate editor coordinating the review of this article and approving it for publication was A. M. Vegni. (Corresponding author: Helin Yang.)

Helin Yang, Liang Xiao, and Yi Zhang are with the School of Informatics and the Key Laboratory of Multimedia Trusted Perception and Efficient Computing, Xiamen University, Xiamen 361005, China (e-mail: helinyang066@xmu.edu.cn; lxiao@xmu.edu.cn; yizhang@xmu.edu.cn).

Sheng Zhang is with the Institute for Infocomm Research, Agency for Science, Technology and Research, Singapore 138632 (e-mail: szhang034@e.ntu.edu.sg).

Arokiaswami Alphones is with the School of Electrical and Electronic Engineering, Nanyang Technological University, Singapore 639798 (e-mail: ealphones@ntu.edu.sg).

Chen Chen is with the School of Microelectronics and Communication Engineering, Chongqing University, Chongqing 400000, China (e-mail: c.chen@cqu.edu.cn).

Kwok-Yan Lam is with the School of Computer Science and Engineering and the Strategic Centre for Research in Privacy-Preserving Technologies, Nanyang Technological University, Singapore 639798 (e-mail: kwokyan.lam@ntu.edu.sg).

Zehui Xiong is with the Pillar of Information Systems Technology and Design, Singapore University of Technology and Design, Singapore 487372 (e-mail: zehui\_xiong@sutd.edu.sg).

Color versions of one or more figures in this article are available at https://doi.org/10.1109/TCOMM.2023.3309823.

Digital Object Identifier 10.1109/TCOMM.2023.3309823

localization accuracy and transmission data rate, compared to existing systems and schemes. Experiments also illustrate that the localization algorithm is more robust against the random tilting of the receiver under device movement in two-dimensional and three-dimensional scenarios.

*Index Terms*— Visible light communication, visible light localization, adaptive transmission, robust scheme, indoor devices.

#### I. Introduction

NDOOR localization is important for object or device positioning, tracking, and navigation in factories, hospitals, airports, offices, train stations, and warehouses [1], [2], [3]. Radio-frequency (RF)-based localization is a typical field of application for indoor localization, tracking and navigation, which has been widely investigated to identify or track the location of mobile objects [2]. However, in indoor RF-based localization systems, the localization accuracy is significantly impaired by indoor multipath reflections and shadowing effects [3], [4].

In recent years, researchers have reported that white light emitting diodes (LEDs) can be installed to set up visible light communications (VLC) systems to support wireless communications and to estimate the locations of mobile devices in indoor environments, such as in office, supermarket, hospital, airport, and factory [2], [3], [4], [5], [6], [7], [8]. Thus, relying on homogeneously deployed lighting infrastructure, VLC-based LEDs has been recently regarded as a potential technique for fifth-generation (5G) communication networks and beyond, as it can not only support illuminations and high-speed communications rate, but also provide high-accuracy localization in indoor environments.

On the one hand, VLC based LEDs is an potential technology for indoor communications with the benefit of high data rate, no RF interference and license-free. The literature [9], [10] provided a fundamental investigation on VLC systems, where the system principle was discussed in detail. After that, the development of VLC has achieved much interests from both academia and industry. The references [11], [12], and [13] presented VLC systems for indoor communication applications, and actual experiments were presented to show the effectiveness of their designed VLC systems in indoor environments. The work in [14] used high-quality LEDs to obtain a data rate of 500 Mbit/s in VLC systems.

In [15], the adaptive modulation designs combining with orthogonal frequency division multiplexing (OFDM) were

0090-6778 © 2023 IEEE. Personal use is permitted, but republication/redistribution requires IEEE permission. See https://www.ieee.org/publications/rights/index.html for more information.

presented in VLC systems to maximize the data rate, where signal-to-noise-ratio (SNR) is acted as a reference to choose modulation levels at different subcarriers. Different optical versions of OFDM were developed for optical communications and the VLC technology, such as optical OFDM [6], asymmetrically clipped optical OFDM [16], DC biased optical OFDM [17], and asymmetrically clipped DC biased optical OFDM [18]. Dissanayake et al. in [17] summarized the advantages of these OFDM techniques and compared their communication performances. Furthermore, the work in [19] and [20] experimentally studied weighted pre-equalization schemes to enhance the communication data rate by compensating frequency attenuation of VLC.

On the other hand, localization and positioning using VLC technology have been proposed to improve the localization accuracy [4], [21], [22], [23], [24], [25], [26], [27], [28], [29], [30], [31], [32] due to the less indoor multipath reflections and shadowing effects compared to RF-based localization. The studies in [4] and [21] provided a comprehensive review of different localization techniques for VLC-based localization, such as received signal strength (RSS), angle of arrival (AoA), time-of-arrival (TOA) and time-difference-of-arrival (TDOA). A real-time indoor positioning systems based on VLC were experimentally demonstrated in [22], where different cell layouts were designed to get the optimum frequency assignment for LED-based coverage. Even though VLC-based localization systems embrace the high-accuracy localization benefit, several fundamental problems in terms of precision, robustness, real-time operation, and reliability remain. For example, VLC-based RSS localization adopts received power to perform location estimation, which is sensitive to background noise and random tilting of photo-detector (PD) plane in a real-world setting [23], [24], [25]. The AoA localization algorithm can achieve high accuracy performance [26], [27], [28] and Li et al. in [26] also demonstrated the localization performance in 3D scenario. The localization algorithms, i.e., TDOA [29] and phase difference of arrival (PDOA) [30], are capable of supporting high-accuracy localization, but they require both expensive synchronized real local oscillators (LOs) and high-speed analog-to-digital converters (ADCs), where these two requirements hinder their practical implementation. Our previously work in [31] presented a hybrid RSS/PDOA scheme to maintain the high localization accuracy under receiver tilting, but it requires a high computational complexity. Recently, Shao et al. [23] proposed an excellent localization scheme achieve nearly 4 cm localization accuracy performance, where a number of PDs (i.e., landmarks) are mounted on any single unmodified light source to sense the retroreflected optical signal (i.e., location signature). Moreover, in addition to providing high-accuracy localization in VLC-based systems, communication services also need to be supported simultaneously in the same system [3], where some indoor scenarios may require high-speed transmission data, e.g., augmented reality (AR) or virtual reality (VR) services need a high-speed transmission data rate up to several hundred megabits per second (Mbps) [32].

Recently, many works presented the integration of VLC and VLL in the same system [3], [33], [34], [35], [36], called

integrated VLCL system, in order to support both communication and positioning applications instead of providing VLC [9], [10], [11], [12], [13], [14], [15], [16], [17], [18], [19], [20], [21], [22] or VLL [23], [24], [25], [26], [27], [28], [29], [30], [31] independently. For example, in a factory, some indoor vehicles need the localization service to transport goods from one place to another place, while some machines require to download images or videos to perform manufacture, and thus the system needs to provide both localization and communication for these devices at the same time in the same system. In detail, the references in [33] and [34] combined orthogonal frequency division multiple access (OFDMA) and RSS in integrated VLCL systems, but the performance is degraded due to severe out-of-band interference generated from OFDM signals. Additionally, an integrated VLCL system applying filter bank multicarrier-based subcarrier multiplexing (FBMC-SCM) was proposed to avoid effect of the out-of-band interference (OOBI) and then improve the system performance [34], [35], but it requires extra computational complexity for signal processing at transmitters. In addition, Yang et al. investigated the resource allocation for integrated VLCL systems with considering quality-of-service (QoS) requirements [36]. Furthermore, considering the negative effect of receiver tilting on the system performance in practical VLL systems, the authors in [25], [33], [36], and [37] provided the analysis of receiver tilting on the localization performance, where the random and unknown tilt angle of receiver can cause significant localization errors when mobile devices move in indoor environments. The works in [25], [33], [36], and [37] used the RSS algorithm to perform localization, where RSS adopts received power to implement location estimation which is greatly sensitive to random tilting of PD plane in a real-world setting. Hence, implementing both communication and real-time indoor localization with high robustness, precision, and reliability is still challenging.

Moreover, there are several new challenges of combining VLL and VLC: 1) Communication bands on the visible light spectrum leak OOBI to adjacent bands, which significantly reduces the communication performance and localization accuracy; 2) There exists a power allocation tradeoff between VLC and VLL, and thus how to effectively allocate fixed or limited transmission power for them to guarantee both the communication and localization requirements is a challenge; 3) light-of-sight (LoS) blocking is an important issue in the integrated system, and how to design a robust handover mechanism to ensure both the communication and localization performance under LoS blockages is also a challenge.

To overcome the challenges mentioned above, this paper experimentally designs an integrated VLCL system (combine OFDMA and a presented advanced differential PDOA (A-DPDOA)) to support both the communication and real-time localization services. A joint adaptive modulation, subcarrier allocation and power allocation design is also proposed to optimize the transmission data rate and localization accuracy of devices. Moreover, different from the work in [1], as RSS-based localization is much sensitive to random tilting of PD plane, an A-DPDOA-based localization algorithm is presented to provide high-accuracy localization. The main contributions of the paper are listed as follows:

- We experimentally design an integrated VLCL system
  to simultaneously support both the communication and
  localization services. The localization signal in integrated
  VLCL system can be used for RSS and A-DPDOA
  localization, and avoid the interference (OOBI) from
  adjacent communication subcarriers.
- An A-DPDOA localization design is developed to simplify hardware without using local oscillators, which reduces the negative effect of hardware on localization accuracy, and improves tracking robustness under receiver tilting. The A-DPDOA localization algorithm can achieve the robust localization accuracy against receiver tilting.
- A joint adaptive modulation, subcarrier allocation and power allocation design is presented to optimize the transmission data rate and localization accuracy performance. In this context, the power allocation tradeoff between VLC and VLL is designed to improve both the communication and localization performances.
- We conduct actual experiments to evaluate the localization accuracy and system data rate performance in practical settings. In detail, centimeter (cm)-level localization/tracking accuracy under device mobility (i.e., the mean 2D tracking error of 4.3 cm and the mean tracking error of 9.3 cm in 3D tracking scenario), as well as data rate of more than one hundred Mbps per unit, are achieved. In addition, compared with other RSS based localization systems, the proposed integrated VLCL system not only achieves higher tracking accuracy, but also is more robust against random tilting of receiver.

*Organization:* The rest of this paper is organized as follows. An advanced integrated VLCL system is shown in Section II. Section III provides the principle of the presented adaptive transmission design. Section IV shows the experimental results and discussion. Section V summarizes the work.

# II. INTEGRATED VLCL SYSTEM MODEL

#### A. Integrated VLCL Framework

As shown in Fig. 1 (a), in addition to supporting indoor light illumination, LED lamps (let 'LED' denote 'LED lamp' in this paper) can be used to set up VLCL systems to support both wireless communication and localization services for indoor devices. At each device, a PD is equipped to receive the optical signal before converting it into electrical signals.

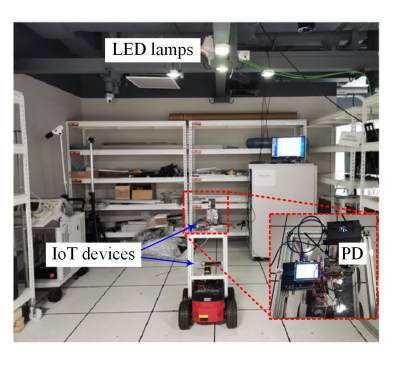
The schema of the system architecture is provided in Fig. 1 (b). At the transmitter side, communication signals and synchronized localization sinewave signals are initially generated from a signal generator, i.e., arbitrary waveform generator. The integrated communication and localization signals are first amplified and then combined with direct current (DC) biases by bias-tees to drive the corresponding LED lamps. At the mobile device side, the receiver consists of an avalanche PD (APD) with an integrated electrical amplifier, a VLC module, and a VLL module. After receiving the optical signals from the LED lamps, the APD converts the optical signal to electrical signals, and then captures them by using an oscilloscope. The Raspberry Pi is used to perform communication signal demodulation, power measurement, and location estimation.

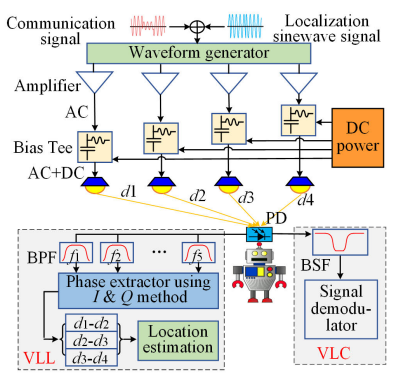
Fig. 1 (c) shows the electronical spectra of integrated communication and localization signals at the LED transmitter sides, which is simulated. Both the communication signal and localization sinewave signal are generated by using MATLAB tool, and they are respectively allocated on the communication subcarriers and localization subcarriers. Then, these two kinds of signal are added together at the LED transmitter side. For the localization module, as illustrated in Fig. 1 (c), the sinusoidal signals with five different frequencies (blue color), i.e., from  $f_1$  to  $f_5$ , are modulated on the four LED lamps. LED lamp 1 carries two sinusoidal signals with frequencies  $f_1$  and  $f_5$ , while LED lamp 2, LED lamp 3, and LED lamp 4 use frequencies  $f_2$ ,  $f_3$ , and  $f_4$  to transmit sinusoidal signals, respectively. Note that these five frequencies are not used to transmit communication signals in one unit of the VLCL system. From Fig. 1(c), it can be seen that there are five frequency holes in the identified subcarriers that have negligible OOBI leakage from adjacent communication subcarriers (red color). In the context, the localization sinusoidal signals (blue color) are put into these frequency holes, to avoid the interference leakage on localization frequency holes from the communication signals. In addition, there exists a power allocation tradeoff between VLC and VLL, and we will design this power allocation scheme to maintain both the communication and localization performances (in Section III).

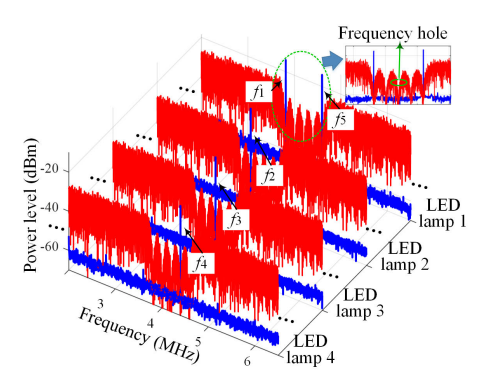
After receiving the mixed integrated communication and localization signals from four LED lamps, band-pass filters (BPFs) and band-stop filter (BSF) are applied to filter both the localization signal and communication signal out from the received mixed signal, respectively. For localization, we propose an advanced differential phase difference of arrival (A-DPDOA) to estimate the location of devices, as it can simplify hardware without using LOs and it is robust against background noise and random tilting of PD plane in real-world settings, where the localization principle of A-DPDOA will be provided in Section II-B.

In the integrated VLCL system, K devices (e.g., robot, machine and phone) randomly distribute on the floor. The system has a central controller, which connects all LEDs to transmit signal to devices. Once the central controller collects the feedback information (e,g., channel information and devices' services), it can schedule the communication and localization tasks. The bandwidth is equally divided into N subcarriers. As each LED lamp has one unique localization subcarrier to transmit localization sinusoidal signal, expect one of them having two unique localization subcarriers in our proposed localization algorithm, totally L+1 subcarriers out of the N subcarriers are applied for localization while ther N-L-1 subcarriers are used for communication. As the system has K devices, there have K communication subcarrier groups (SGs).

The power allocation tradeoff between VLC and VLP, and the interference (OOBI) will affect each other. When the transmission power of LED is fixed, if the VLCL system allocates more power to VLC spectrum subcarriers, the system can achieve the higher communication data rate, but the positioning subcarriers will be allocated with less power and the localization accuracy will decrease in this case. In contrast,







(a) Experiments conducted set up

(b) Block diagram of the integrated system.

(c) Electrical spectra of the integrated signal

Fig. 1. The system model of integrated VLCL system.

if the system allocates more power on positioning subcarriers, the locations accuracy can be improved due to the high received signal strength, but the communication data rate will decline due to the less received signal power. Thus, there exists some tradeoff between them in term of power allocation.

#### B. Communication Model

In integrated VLCL system, the received SNR at device k on communication subcarrier n is expressed as

$$\gamma_{k,n}^{\text{co}} = \mu^2 \left( \sum_{i=1}^{L} \sqrt{P_{n,i}} H_{i,n,k} \right)^2 / \delta^2,$$
 (1)

where  $\mu$  denotes the PD's responsivity.  $P_{n,i}$  represents the allocated electrical power on subcarrier n at LED i.  $H_{i,n,k}$  is the line-of-sight (LoS) optical channel gain from LED i to device k on subcarrier n.  $\delta^2$  denotes the additive background noise power at the devices [6], [9].

For device k, if it is assigned on the n-th subcarrier, the transmission signal can be modulated by  $M_n$ -quadrature amplitude modulation (QAM) with the modulation order  $M_n$ , the bit error rate (BER) is defined by adopting [6], [9],

$$BER_{k,n} = \frac{\sqrt{M_n} - 1}{\sqrt{M_n} \log_2(\sqrt{M_n})} erfc\left(\sqrt{\frac{3\gamma_{k,n}^{\text{co}}}{2(M_n - 1)}}\right). \quad (2)$$

The transmission data rate (bits/s) of the *k*-th device on its assigned subcarrier can be given by [6], [9], [10], [11], [12], and [13]

$$R_k = B_{sub} \sum_{n=1}^{N/2-1} (\rho_{k,n} \log_2 M_n), \tag{3}$$

where  $\rho_{k,n}$  denotes a binary parameter,  $\rho_{k,n} \in \{0,1\}$ , and  $\rho_{k,n} = 1$  shows that the communication subcarrier n is allocated to device k; otherwise,  $\rho_{k,n} = 0$ .  $B_{sub}$  denotes subcarrier bandwidth  $B_{sub} = B/N$ , where B denotes the transmission bandwidth.

# C. Proposed A-DPDOA Localization

Let  $d_{i,k}$  denotes the transmission distance between the *i*-th LED lamp and the *k*-th device, we have  $d_{i,k} = t_{i,k}c$  with c being the speed of light and  $t_{i,k}$  being the corresponding propagation time. The propagation time  $t_{i,k}$  can be given by:

 $t_{i,k} = \Delta \varphi_{i,k}/2\pi f_i$ , where  $\Delta \varphi_{i,k}$  is the phase shift of the transmitted sinusoid signal at the frequency of  $f_i$  for device k. With reference to Fig. 1 (c), let  $S_i^{\mathrm{Tx}}(t)$  denote the input sinusoidal signal modulated on the i-th LED lamp, which is expressed as

$$S_i^{\text{Tx}}(t) = \sqrt{P_i}\sin(2\pi f_i t + \varphi_0),\tag{4}$$

where  $\varphi_0$  is the initial phase of the signal. After propagating through an indoor optical wireless channel, being detected and passing through a BPF, the received signal  $S_i^{\rm Rx}(t)$  at the k-th device is given by

$$S_{i,k}^{\text{Rx}}(t) = \sqrt{P_i} H_{i,k} \sin(2\pi f_i t + \Delta \varphi_{i,k} + \varphi_0) + n_k(t), \quad (5)$$

where  $n_k(t)$  is the background noise at device k, and  $H_{i,k}$  is the LOS optical wireless channel gain between device k and the i-th LED lamp. To measure  $\Delta \varphi_{i,k}$ , an I/Q (In phase and Quadrature) demodulator is required. However, this method requires a LO to generate a reference signal at the frequency  $f_i$  with a phase locked loop (PLL) circuit to decode the phase shift  $\Delta \varphi_{i,k}$ . This LO needs to precisely synchronize the transmitted sinusoidal signal, which significantly increases the system complexity and affects the measurement accuracy, since there are multiple VLL lamps. In this work, we propose a non-LO based differential phase-shift measurement to obtain  $\Delta \varphi_{i,k}$ , which can be used in the triangulation algorithm for the localization estimation. Equation (5) can be re-written as

$$S_{i,k}^{\mathrm{Rx}}(t) = \sqrt{P_i} H_{i,k} \sin(\omega_i t + \omega_i t_{i,k} + \varphi_0) + n_k(t). \tag{6}$$

where  $\omega$  is the angular frequency:  $\omega = 2\pi f$ . To extract the implicit parameter  $d_{i,k}$  from equation (6), we use a differential phase shift measurement approach. Multiplying  $S_1^{\rm Rx}(t)$  by  $S_2^{\rm Rx}(t)$ , we have

$$S_{1,k}^{\text{Rx}}(t)S_{2,k}^{\text{Rx}}(t) = -\frac{1}{2}\sqrt{P_1}\sqrt{P_2}H_{1,k}H_{2,k}$$

$$\times \left[\cos\left((\omega_1 + \omega_2)t + \omega_1 t_{1,k} + \omega_2 t_{2,k} + 2\Delta\varphi_0\right) - \cos\left((\omega_2 - \omega_1)t + \omega_2 t_{2,k} - \omega_1 t_{2,k}\right)\right] + n_{12,k}(t), \tag{7}$$

where  $n_{12,k}(t)$  is the additive noise term. After the received signal passing through a BPF with center frequency of

 $(\omega_2-\omega_1)$  and noise being ignored, the phase difference related term is achieved by

$$D_{1,k}(t) = \frac{1}{2} \sqrt{P_1} \sqrt{P_2} H_{1,k} H_{2,k} \cos((\omega_2 - \omega_1)t + \omega_2 t_{2,k} - \omega_1 t_{1,k}),$$
(8)

Similarly, we have

$$D_{i,k}(t) = \frac{1}{2} \sqrt{P_i} \sqrt{P_{i+1}} H_{i,k} H_{i+1,k} \times \cos((\omega_{i+1} - \omega_i)t + \omega_{i+1} t_{i+1,k} - \omega_i t_{i,k}),$$

$$\times i = 2, 3, 4.$$
(9)

Multiplying equations (8) by (9), when we take  $D_{1,k}(t) \times D_{2,k}(t)$  as an example, the differential expression is then obtained, i.e.,

$$D_{1,k}(t) \times D_{2,k}(t) = \frac{1}{8} \sqrt{P_1} P_2 \sqrt{P_3} H_{1,k} H_{2,k}^2 H_{3,k}$$

$$\times \left[ cos((\omega_3 - \omega_1)t - \omega_1 t_{1,k} + \omega_3 t_{3,k}) + cos(\omega_1 t_{1,k} + \omega_3 t_{3,k} - 2\omega_2 t_{2,k}) \right]$$

$$(10)$$

To achieve the differential of phase differences (DPDs), the phase of  $D_{1,k}(t) \times D_{2,k}(t)$  should be extracted. We can respectively extract the In-Phase and Quadrature-phase components by adopting

$$I_{1,k} = LPF (D_{1,k}(t) \times D_{2,k}(t))$$

$$= \frac{1}{8} \sqrt{P_1} P_2 \sqrt{P_3} H_{1,k} H_{2,k}^2 H_{3,k} \cos$$

$$\times (\omega_1 t_{1,k} + \omega_3 t_{3,k} - 2\omega_2 t_{2,k}), \qquad (11)$$

$$Q_{1,k} = LPF (D_{1,k}(t) \times Hilb (D_{2,k}(t)))$$

$$= \frac{1}{8} \sqrt{P_1} P_2 \sqrt{P_3} H_{2,k}^2 H_{3,k} \sin$$

$$\times (\omega_1 t_{1,k} + \omega_3 t_{3,k} - 2\omega_2 t_{2,k}), \qquad (12)$$

where  $LPF(\cdot)$  and  $Hilb(\cdot)$  are LPF and the Hilbert transformation, respectively. Taking ratio as  $Q_{1,k}/I_{1,k}$ , the amplitude terms are canceled, leading to a  $\tan(\cdot)$  based phase term. Extracting the dual differential of phases with, we have

$$\omega_1 t_{1,k} + \omega_3 t_{3,k} - 2\omega_2 t_{2,k} = \tan^{-1} \left( Q_{1,k} / I_{1,k} \right).$$
 (13)

Similarly, we also have

$$\omega_2 t_{2,k} + \omega_4 t_{4,k} - 2\omega_3 t_{3,k} = \tan^{-1} (Q_{2,k}/I_{2,k}),$$
 (14)

$$\omega_3 t_{3,k} + \omega_5 t_{1,k} - 2\omega_4 t_{4,k} = \tan^{-1} (Q_{3,k}/I_{3,k}).$$
 (15)

Note that we set that the five localization frequencies are the arithmetic progression, then the above equation groups from equation (13) to (15) can be solved by the following matrix

$$\begin{pmatrix} d_{1,k} - d_{2,k} \\ d_{2,k} - d_{3,k} \\ d_{3,k} - d_{4,k} \end{pmatrix} = c \begin{pmatrix} \tan^{-1}(Q_{1,k}/I_{1,k}) \\ \tan^{-1}(Q_{2,k}/I_{2,k}) \\ \tan^{-1}(Q_{3,k}/I_{3,k}) \end{pmatrix} \times \begin{pmatrix} \omega_1 - \omega_3 & 0 \\ 0 & \omega_2 & -\omega_4 \\ \omega_5 & \omega_5 & \omega_5 + \omega_3 \end{pmatrix}^{-1}, \quad (16)$$

where  $t_{i,k}$  is replaced by  $d_{i,k}$  and c using  $t_{i,k} = d_{i,k}/c$ , and  $\tan^{-1}(Q_{i,k}/I_{i,k})$  can be calculated after measuring the

parameters in the experiment. Considering  $d_{i,k} - d_{i+1,k}$  as a variable, we get a rank equations which can effectively address these distance differences variables problem. To compute the k-th device's location  $(x_k, y_k, z_k)$ , the relationship between the receiver location and the transmission distance is  $d_{i,k} = \sqrt{((x_i - x_k)^2 + (y_k - y)^2 + (z_k - z)^2)}$ , where

is  $d_{i,k} = \sqrt{((x_i - x_k)^2 + (y_k - y)^2 + (z_k - z)^2)}$ , where  $(x_i, y_i, z_i)$  denotes the poistion of the LED lamp i. From Eq. (11), (12), and (16), we can observe that the distance deference variable  $d_{i,k} - d_{i+1,k}$  is determined by both the In-Phase  $I_{i,k}$  and the Quadrature-phase  $Q_{i,k}$ , and these two components  $I_{i,k}$  and  $Q_{i,k}$  are related to the transmission power  $P_i$ . Thus,the selection of transmission power value affects the distance deference variable estimation accuracy, and finally affects the localization error.

Conventionally, the receiver can apply the Newton-Raphson and Levenberg-Marquard schemes to numerically complete the location estimation. However, these solutions require much longer computational time than expected if the initial values are inappropriately selected. Moreover, it should be noted that there exist relatively location shifting errors in the localization system due to the following two factors: 1) the VLCL hardware may have bias errors of time delay measurements when we implement the experiments; 2) the calibration process on Initial Time Delay (ITD) at all LED lamps. To address these issues, the shifting error mitigation technique is adopted to simplify the trilateration solution and improve the location accuracy.

# III. ADAPTIVE TRANSMISSION DESIGN FOR INTEGRATED VLCL SYSTEMS

The block diagram of the adaptive transmission scheme for the integrated VLCL system is illustrated in Fig. 2, where a joint adaptive modulation, subcarrier allocation as well as power allocation is presented to improve the localization accuracy and communication performance. The process to realize the adaptive transmission are provided by the following analysis.

At the transmitters, the system allocates communication SGs to devices, and then the localization signals for VLL are integrated with communication signal at all LEDs, where five localization frequencies from  $f_1$  to  $f_5$  are set into the (K+1)-th SG and all communication signals are allocated on K SGs. The central controller receives the information (e.g., channel state information, channel quality, and data rate requirements) from devices, and it selects the adaptive M-QAM mapping according to devices' different minimum data requirements and feedback information.

According to (1), the system chooses the modulation order  $M_n$  based on the SNR value  $\gamma_{k,n}^{co}$  of device k, which is

$$M_n = 2^j, \quad \gamma_j^{\text{th}} \le \gamma_{k,n}^{\text{co}} \le \gamma_{j+1}^{\text{th}}, \ j = 1, \dots, J - 1,$$
 (17)

where  $\gamma_j^{\rm th}$  denotes the SNR target value of the corresponding modulation level j, its current  $BER_{k,n}$  should be less than the maximum tolerant threshold  $BER_{max}$ . The above analysis in (17) shows the modulation order selection process based on the received SNR information from devices.

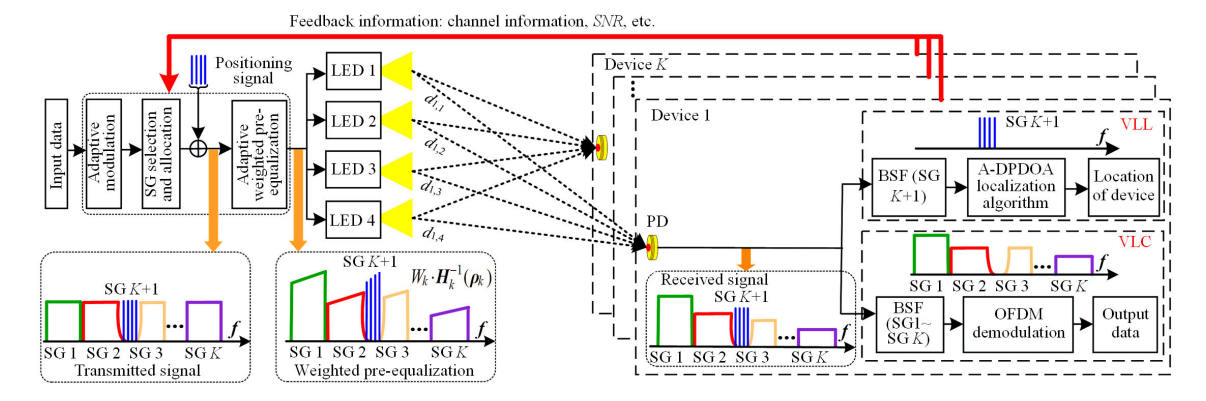


Fig. 2. Block diagram of the proposed adaptive transmission for integrated VLCL systems.

Considering the fact that the severe attenuation of LEDs in high frequency domain in optical systems, the power allocation based on pre-equalization method is adopted to compensate the frequency attenuation at LED sides. We find that transitional pre-equalization methods are not optimal, because the system sacrifices a large amount of power to balance of the attenuation in high frequency domains. The authors in [15], [19], and [20] proposed a power allocation based on pre-equalization scheme to optimize the sum data rate of all subcarriers. However, power allocation schemes in [15], [19], and [20] was still not the optimal scheme, because it is only a fixed-order modulation as well as static subcarrier allocation. Therefore, the joint adaptive transmission design is presented to dynamically improve the transmission data rate while ensuring the localization accuracy requirement.

The modulation order of the k-th SG is denoted by  $M_k$ . The continuous subcarrier allocation indicator for device k is denoted by  $\rho_k$ . In addition, the k-th SG signal in the frequency domain when considering the joint adaptive modulation, subcarrier allocation, as well as power allocation is expressed as

$$\boldsymbol{S}_{k}'(M_{k}, \boldsymbol{\rho}_{k}) = \sqrt{P_{k}} \cdot \boldsymbol{H}_{k}^{-1}(\boldsymbol{\rho}_{k}) \cdot \boldsymbol{S}_{k}(M_{k}, \boldsymbol{\rho}_{k}),$$
 (18)

where  $S_k'(M_k, \rho_k)$  and  $S_k(M_k, \rho_k)$  are the k-th SG signal vector before and after pre-equalization, respectively.  $P_k$  and  $\boldsymbol{H}_k$  denote the power allocation coefficient on the k-th subcarrier group and the transfer function matrix of SG k, respectively. Note that  $H_{i,k}$  is one subcarrier of the subcarrier group  $\boldsymbol{H}_k$ . It is worth noting that  $\boldsymbol{H}_k$  is a diagonal matrix.  $\boldsymbol{H}_k$  can be measured offline before the experiment.

At each device, for VLL, the received localization signal on the five localization frequencies from four corresponding LEDs can be measured in the integrated VLCL system by using band stop filter (BSF). After obtaining the four received localization power levels, the location of the device is achieved by adopting the A-DPDOA-based localization algorithm. For VLC, the communication signals are achieved when the received signals are filtered by using BSF, and finally communication signals are demodulated by adopting OFDM demodulation technique.

Note that for the channel feedback issue, in general communication systems, it also needs receiver to send its channel information to the transmitter. When we consider the auto-rate function, the receiver needs only to feed back its received SNR to the transmitter for the system data rate update. When the SNR value is sent back, we can know whether the data rate can meet the QoS requirement or not. If it fail to meet the QoS requirement, we can use the water-fulling method to increase power allocation value in the next iteration to enhance the achievable data rate.

For the localization algorithm design, let G denote the sample points of each received localization signal. The system uses filter to flit the five signals in equation (5) and four signals in equation (9), which respectively require about the computational complexity of 5GlogG and 4GlogG [35]. The computational complexity in Eq. (7) and (10) are 4G and 3G, respectively. The computational complexity of Eq. (11) and (12) is about 6G. The computational complexity in the location derivation in Eq. (16) is about  $L^{2.5} \ln(1/\kappa)$ , where  $\kappa$  is the iteration tolerance and L is the number of LED lamps. According to the above analysis, the experimental computational complexity of the localization algorithm is  $O\left(9G + 9G\log G + L^{2.5}\ln(1/\kappa)\right)$ .

The joint optimization algorithm can be summarized as follows:

**Step 01:** Initialize the iteration i=0, set the sum data rate  $R_{\text{sum}}(0) = 0$ , subcarrier allocation indicator  $\rho_k(0)$ , weighted pre-equalization coefficients  $P_k(0)$  and the modulation order  $M_k(0)$  of each device. Set the maximum tolerance  $\varsigma \geq 0$ ;

**Step 02:** Each device k sends its detected channel information, localization accuracy requirements and minimum data rate requirements  $R_k^{\min}$  (QoS requirement) to the transmitter side by WiFi or VLC uplink links;

**Step 03:** The transmitters update the weighted preequalization coefficients  $P_{K+1}(0)$  on positioning SG to guarantee localization accuracy first;

**Step 04:** According to the device's minimum data rate requirements, the transmitter iteratively calculates subcarrier allocation indicator  $\rho_{k}(0)$ , weighted pre-equalization coefficients  $P_{k}(i+1)$  and modulation order  $M_{k}(i+1)$  for devices, to satisfy their minimum data rate requirements first, in other work, allocating communication resource to satisfy  $R_{k}(i) \geq R_{k}^{\min}$  for each device;

**Step 05:** After ensuring the minimum data rate requirements of devices, the system allocates the extra power and subcarriers

to the devices with best channel quality to maximize  $R_{\mathrm{sum}}(i+1)$  by updating  $\rho_k(i+1)$ ,  $P_k(i+1)$  and  $M_k(i+1)$ . For example, the water-filling method is used to allocate the number of available subcarriers to each device to meet its minimum data rate constraint. After allocating a part of subcarriers to all devices to guarantee their QoS requirements, the extra subcarriers will be allocated to the devices who have higher channel gains to maximize the system sum data rate.

**Step 06:** Set i = i + 1, and then update the sum data rate  $R_{\text{sum}}(i)$ ;

**Step 07:** Repeat Step 02 to Step 06 until  $|R_{\text{sum}}(i) - R_{\text{sum}}(i-1)| \le \varsigma$ ;

**Step 08:** Output the parameters  $\rho_k(i)$ ,  $P_k(i)$  and  $M_k(i)$ .

Note that the above joint optimization algorithm uses the water-filling method to allocate both power and subcarrier to guarantee devices' minimum data rate constraints and maximize the system sum data rate, and the method will converge to a sub-optimality.

#### IV. EXPERIMENTAL SETUP AND RESULTS

Fig. 1(b) illustrates the lighting system, which is used to evaluate the localization accuracy and communication data rate performances. We demonstrate the experiment with a coverage area of 222.5  $m^3$ . We set the locations of four LEDs as (-0.4, 0.4, 1.35), (0.4, 0.4, 1.35), (-0.4, 0.4, 1.35) and (-0.4, -0.4, 1.35) in meters. The Inverse Fast Fourier Transform (IFFT) size N=256. The modulation bandwidth we use is 20 MHz. The modulation order  $M = \{2, 4, 8, 16, 32, 64\}$ and  $BER_{\rm max} = 3.8 \times 10^{-3}$ . The frequencies of the five sinusoidal signals for localization range from 4.0 to 4.8 MHz with each frequency gap being 0.2 MHz. Generally, the 2D localization service of the proposed localization needs at least three LED lamps, and the 3D localization service of the proposed localization needs at least four LED lamps. Generally, the 2D localization service of the proposed localization scheme needs at least three LED lamps, and the 3D localization service of the proposed localization scheme needs at least four LED lamps. In the manuscript, as its an experimental setting up, we use four LED lamps to demonstrate the performance.

From Fig. 1(b), we provides the experimental setup to show the communication localization performance. The PD equipped with each device is put at the top of the robot or indoor vehicle. In this case, one of our researchers move it during the experiment process. In order to avoid blocking the visible light at the receiver, the research is on hands and knees to perform the experiments. The movement trajectory is planned before the experiment, which is shown in Fig.6 and Fig. 7 with blue color. When implementing the experiment, the research carefully pushes the robot along the planned trajectory, the location estimation can be obtained by the Rasperry Pi and computer.

# A. Online Localization Delay Evaluation

To show the computation latency of localization, we compare the computation time of the the proposed A-DPDOA-based localization scheme with the Newton-Raphson-based localization scheme, which is illustrated in Fig. 3. The online

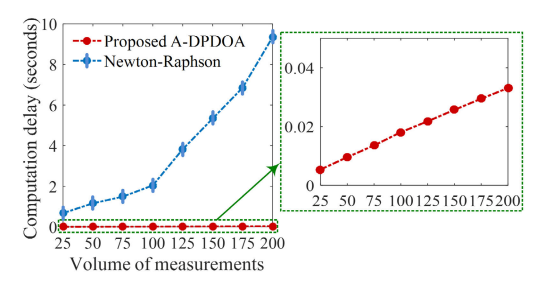


Fig. 3. Online localization delay evaluation.

computation time of the existing Newton-Raphson scheme is significantly reduced by one order of magnitude by applying the A-DPDOA-based localization. In detail, when the volume of the localization measurements are 100, the online computational time of the A-DPDOA-based is decreased from about 2.0 second (s) to 0.018 s, while this value can be reduced from 9.30 s to 0.03 s when the volume of the measurements are 200. For the A-DPDOA and Newton-Raphson-based schemes, the average computation times of one localization measurement are 0.0015 s and 0.019 s, respectively. As these two schemes need to process localization signal at the PD, and the additional signal processing time is 0.0186 s. We would like to mention that the computational time illustrated in Fig. 3 is only the online processing latency, and the results verify that the proposed A-DPDOA-based localization scheme can obviously save computational time compared with the Newton-Raphson scheme. Therefore, the presented A-DPDOA-based localization can perform real-time indoor localization for the scenarios where low-latency services are required.

#### B. 2D/3D Localization Performance of A-DPDOA

Fig. 4(a)-(c) represents the 2D localization results applying A-DPDOA at three height levels of 1.2 m, 1.5 m, and 1.8 m, respectively. Here, the vertical height from the LED lamps plane to the PD plane is denoted as h. We find that the low localization estimation errors are achieved when mobile devices are located near the center. However, once the devices are far away from the center, it can be seen that the localization estimation errors increase up to 10 cm, because the location estimations suffer from shifting errors due to the time delay measurements of the bias hardware and the calibration process on the ITD at all LED lamps. The shifting error is common in general VLC systems which results from the instability of the measurement equipment. However, the shifting errors can be solved by applying our previously presented shifting mitigation algorithm [30], and thus these large localization errors caused by shifting are effectively mitigated. The mean 2D location estimation errors at three heights of 1.2 m, 1.5 m, and 1.8 m are 4.8 cm, 5.9 cm, and 6.7 cm, respectively.

We also evaluate the localization error performance in 3D scenario at three heights, i.e., 1.2 m (Fig. 4(d)), 1.5 m (Fig. 4(e)), and 1.8 m (Fig. 4(f)), which are unknown to the receiver. As the 3D localization environment is more complex than that of 2D localization, the localization results shown in Fig. 3 are worse than those of Fig 4(a)-(c). The mean location estimation errors at the heights of 1.2 m, 1.5 m, and 1.8 m are

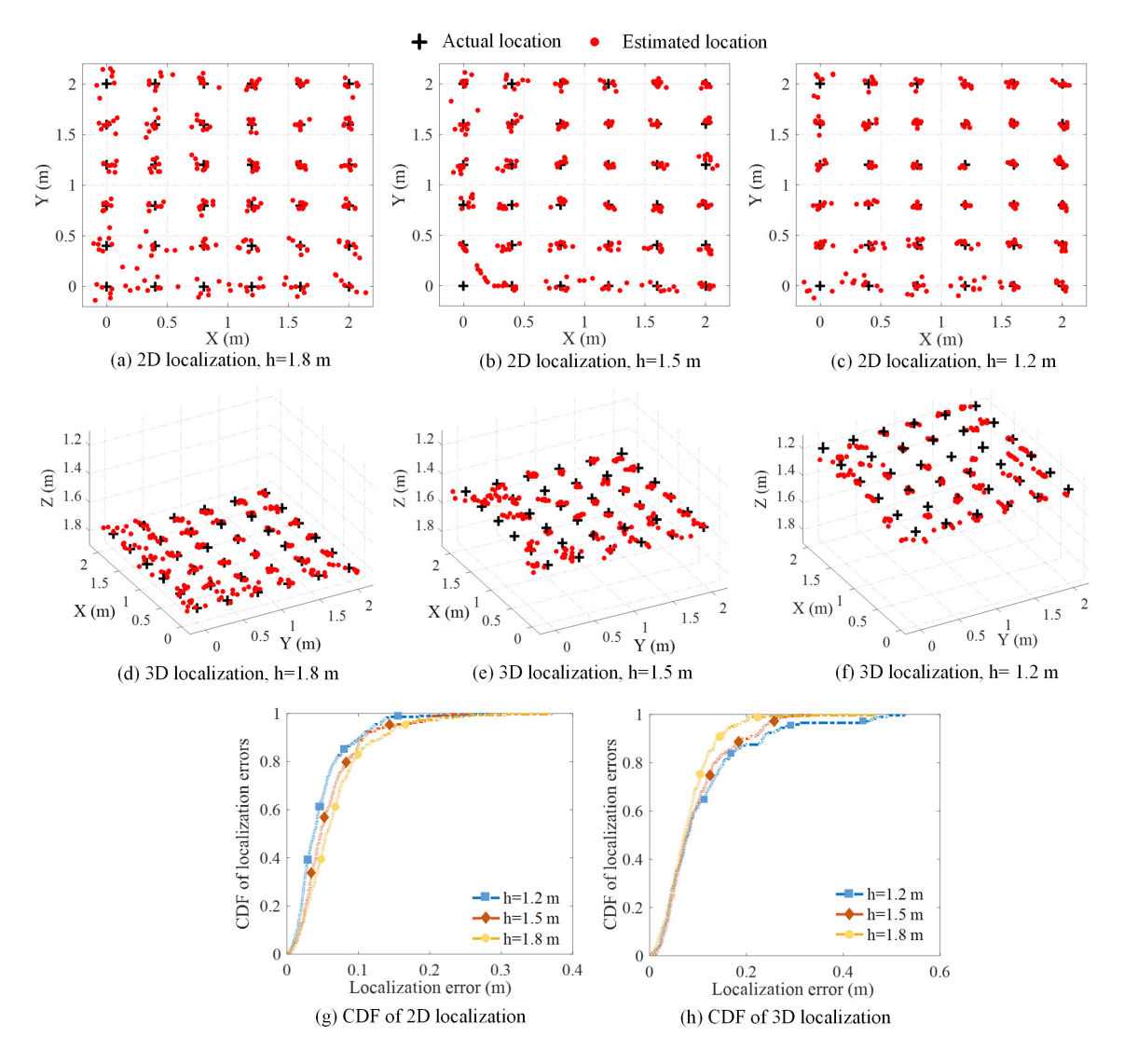


Fig. 4. Comparisons of localization results and localization errors' CDF.

10.8 cm, 9.5 cm, and 8.0 cm, respectively. Fig. 4(g) shows the Cumulative Distribution Function (CDF) of the 2D localization error distributions of Fig. 4(a)-(c).

From Fig. 4(g), we find that when the vertical height is 1.5 m, the location errors are less than 10 cm in 90%. The CDF of 3D location errors of Figs. 4(d)-(f) is provided in Fig. 4(h), where the localization errors are less than 20 cm in 90% at the height of 1.5 m. These results verify that the high localization accuracy of A-DPDOA in both 2D and 3D localization environments.

#### C. Performance Evaluations Under PD Random Tilting

Here, we evaluate the localization robustness of the proposed A-DPDOA-based localization and the existing RSS-based localization [1], [23], [24], [25]. As shown in Fig. 5(a), the PD plane can maintain at a horizontal level when the indoor ground is absolutely smooth. However, when some areas of the indoor ground are uneven, the PD plane tilts to a certain degree which decreases the receiver signal strength

transmitted from some LED lamps, and finally degrades the localization performance. As illustrated in Fig. 5(b), two tests each of 8 measurements at one fixed location at the coordinate (0.4 m, 2 m, 1.5 m) are conducted with PD plane tilting, where the measurements of A-DPDOA distance difference and received RSS amplitude are provided in this figure. Note that the first 4 measurements are under the normal condition with the PD plane being horizontal, while the next 4 measurements are under PD plane tilting. The PD plane tilting randomly ranges from 10 degree to 20 degree in these measurements. We can easily observe that both A-DPDOA and RSS measurements are affected by the random tilting of PD plane, and RSS measurements are more sensitive to PD plane tilting than that of A-DPDOA. For example, the received RSS amplitude significantly changes from 40 millivolt (mV) of horizontal PD plane to about 20 mV of PD plane tilting, while the distance difference of A-DPDOA only changes from 2.6 m to 2.7 m during this process.

Fig. 5(c) illustrates the localization results of the proposed A-DPDOA-based localization and the existing RSS-based

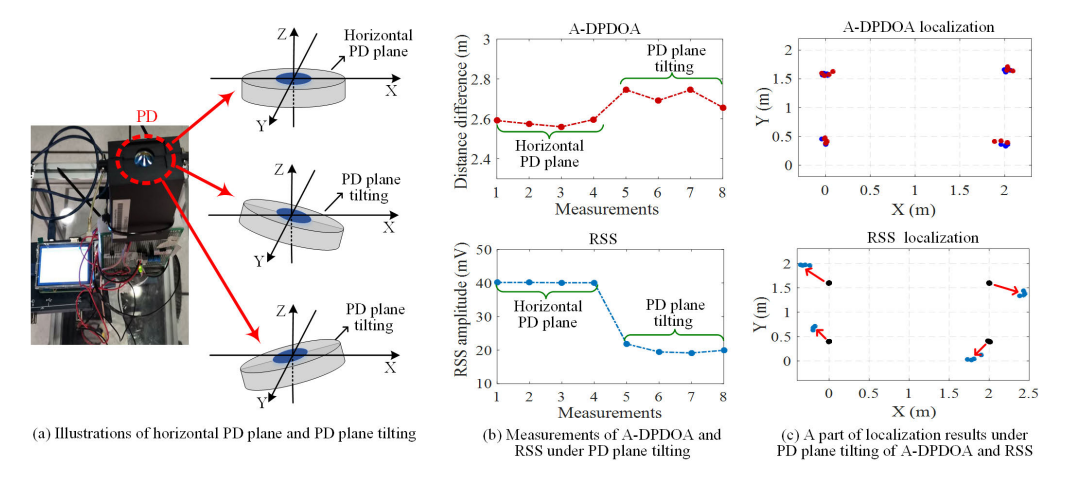


Fig. 5. Measurements under random tilting of PD plane.

localization [1], [23], [24], [25] under PD plane tilting. The blue dots and black dots show the normal measurements under horizontal PD plane of A-DPDOA and RSS, respectively, the dark red dots present the localization results of A-DPDOA under PD plane tilting, and the blue dots show the localization results of RSS under PD plane tilting. As depicted in Fig. 5(c), the estimated locations (dark red dots) of A-DPDOA are very close to the actual locations in the presence of PD plane tilting, while the estimated locations (blue dots) of RSS deviate from the actual locations in this case. The reason lies in the fact that when the PD plane tilts, the current measurements of the received signal power from all LED lamps deviate from the actual measurements, where the RSS utilizes the measured received power strength to perform localization which is relatively sensitive to the PD plane tilting [25], [33], [36], and [37], while A-DPDOA measures the phase difference between LED lamps and the PD instead of received power strength which is less sensitive to PD plane tilting. The experimental results have verified that the proposed A-DPDOA-based localization can obtain higher robustness than that of the RSS-based localization against PD plane tilting.

#### D. 2D Tracking Comparisons of A-DPDOA and RSS

To demonstrate the real-time indoor tracking performance, we experimentally replayed the 2D estimated trajectories of the proposed A-DPDOA-based localization and the existing RSS-based localization [1], [23], [24], [25] at the vertical height of 1.5 m shown in Fig. 6(a). From Fig. 6(b), we can easily observe that the estimated trajectory of the proposed A-DPDOA-based localization is very close to the actual trajectory of the mobile robot, while the estimated trajectory of the existing RSS-based localization (Fig. 6(c)) significantly deviates from off the actual trajectory in some areas. The reason lies in the fact that the uneven indoor ground leads to the mobile devices to shake and thus the PD plane tilts sometimes. Once the PD plane tilts, the current measurements of the received power from all LED lamps deviate from the actual measurements. The RSS-based localization utilizes the measured received power strength to perform localization which is relatively sensitive to the PD plane tilting, while

A-DPDOA-based localization measures the phase difference between LED lamps and the mobile devices instead of received power intensity or power strength which is less sensitive to movement shake. Thus, the tracking accuracy of A-DPDOA is quite higher than that of RSS under the device movement, especially at the edge or corner areas. For example, the mean 2D tracking errors of A-DPDOA and RSS are 4.3 cm and 18.2 cm, respectively.

The 2D tracking errors of A-DPDOA and RSS with respect to each traveling time step at the height of 1.5 m are provided in Fig. 6(d). From Fig. 6(d), we can observe that large tracking errors of RSS are sometimes generated during traveling, and the tracking performance frequently fluctuates with different traveling steps. The reason lies in the fact that the measured received power strengths from all LED lamps deviate from the actual values when the PD plane tilts under movement. However, A-DPDOA is less sensitive to the PD plane tilting as it adopts the phase difference of arrival to perform localization instead of received power strength. Fig. 5(e) compares the cumulative tracking errors of A-DPDOA and RSS under device movement. Obviously, at 90% of the CDF confidence, the tracking errors of the two localization algorithms are around 9.8 cm and 43.5 cm, respectively. The largest tracking errors of A-DPDOA and RSS are around 15.4 cm and 51.0 cm, respectively. The experimental results clearly demonstrate that the tracking errors of RSS is too large to be considered under device movement, while A-DPDOA is capable of robustly tackling real-world tracking problems with high tracking accuracy.

#### E. 3D Tracking Comparisons of A-DPDOA and RSS

Considering the fact that some devices may require 3D tracking services, we further evaluated the 3D tracking performance of A-DPDOA and RSS, shown in Fig. 7. In each measurement, the vertical height between the PD plane and LED lamps plane ranges from 1.2 m to 1.8 m, and the 3D trajectory of the PD is in the 3D space (light blue space) shown in Fig. 7(a). Different from 2D tracking scenario, the 3D trajectory is complex and may limit the tracking accuracy improvement. As shown in Fig. 7(b), A-DPDOA can still

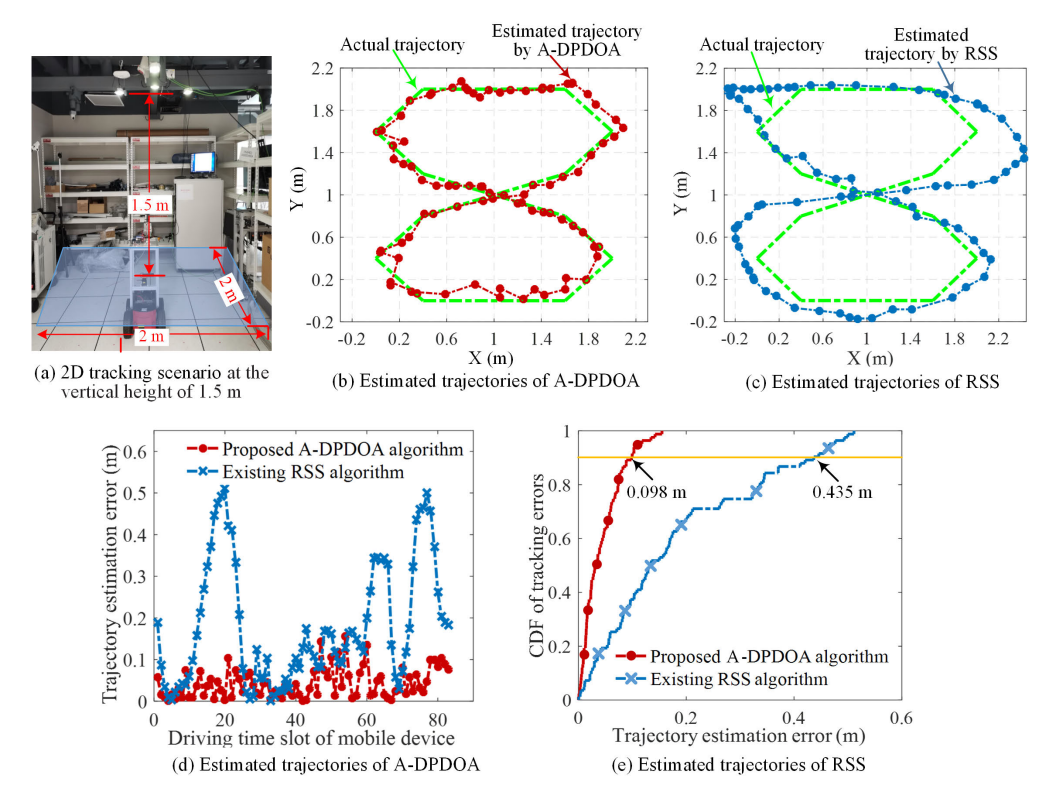


Fig. 6. 2D tracking measurements under random tilting of PD plane.

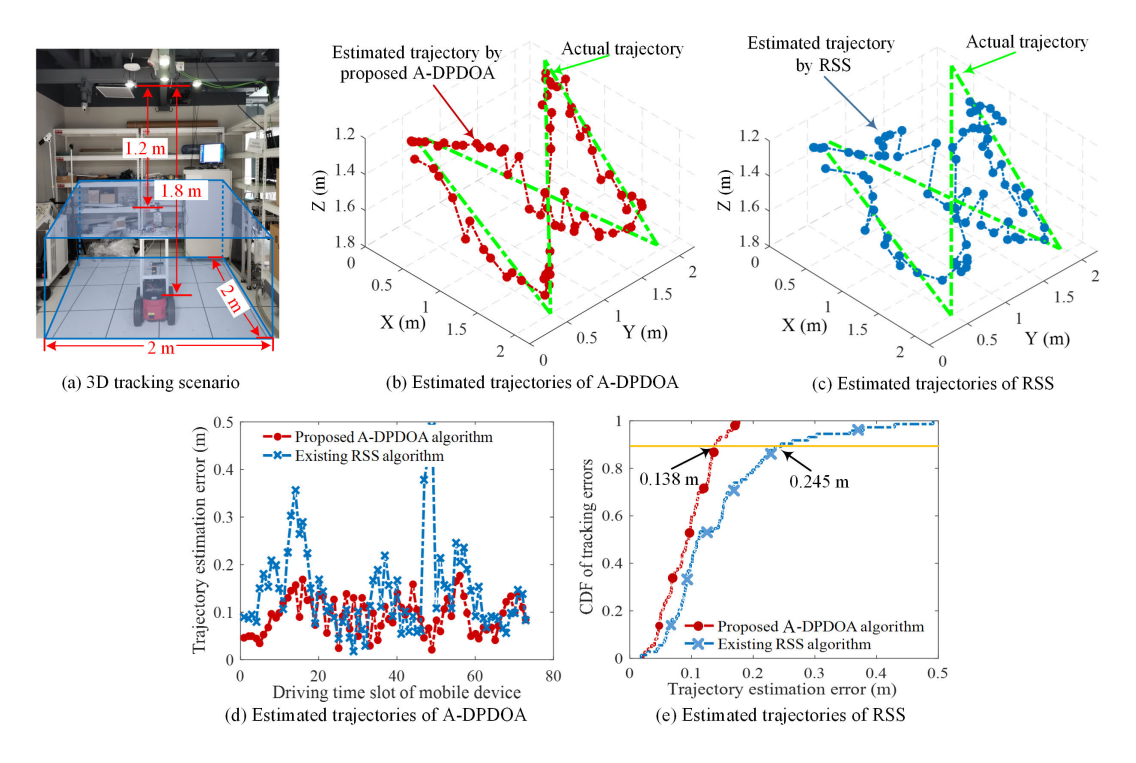


Fig. 7. 3D tracking measurements under random tilting of PD plane.

maintain good 3D tracking accuracy under robot movement through suppressing the tracking error caused by uncertain PD plane shake under the device mobility, while RSS (Fig. 7(c)) deviates from the actual trajectory sometimes due to the PD plane shake. The average 3D tracking errors of A-DPDOA and RSS are 0.093 m (9.3 cm) and 0.145 m (14.5 cm), respectively.

The 3D tracking errors of A-DPDOA and RSS with respect to each traveling time step are provided in Fig. 7(d). As 3D tracking environment is complex, large 3D tracking errors (up to 0.2 m tracking error) of RSS were frequently generated in cases when the PD plane tilting happens. By contrast, this negative issue can be effectively addressed by

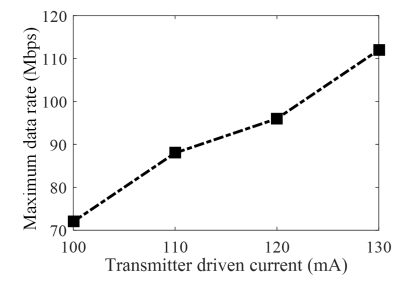


Fig. 8. Communication data rate in one unit area.

using A-DPDOA, which can support stable tracking accuracy against random tilting of PD plane under the device movement. The cumulative 3D tracking errors of two localization algorithms were conducted in Fig. 7(e). For our proposed A-DPDOA-based localization, its cumulative 3D tracking error (Fig. 7(c)) is higher than that of 2D tracking error (Fig. 6(e)) due to a complex environment. However, the lower 3D tracking error can be achieved by A-DPDOA compared with RSS even the mobile device executes a complex trajectory. In Fig. 6(e), the tracking errors of A-DPDOA are less than 0.138 m (13.8 cm) in 90 percent of the cases while the tracking errors of RSS are around 0.245 m (24.5 cm). For the comparison of the tracking results shown in Fig. 6 and Fig. 7. the underlying reason for the superiority of the proposed A-DPDOA-based localization in tracking accuracy is the ability to improve the tracking robustness against movement shake.

#### F. Communication Performance of VLCL System

Finally, the indoor communication performance of the proposed integrated VLCL system was investigated. Fig. 8 shows the data rate at  $2\times 2$  m² area as a function of driven current for LED lamps. Obviously, as the driven current increases, the system data rate enhances due to the increased received power at the PD. A maximum data rate of 112 Mbps is achieved for a driven current of 130 mA with an available modulation bandwidth of 20 MHz when the distance from devices to the LED lamp is 1.5 m.

Fig. 9 illustrates the total transmission data rate of all devices and the QoS satisfaction level under different input current levels for the three schemes. When the input current increases, both the system data rate and the QoS satisfaction performance are improved due to the increased received signal power at devices. Our proposed joint optimization scheme (joint power allocation, subcarrier allocation and adaptive modulation) outperforms the joint power allocation and adaptive modulation scheme in [39], because the system optimizes subcarrier allocation. By contract, the scheme in [40] achieves the worse data rate performance, the reason is that it has low bandwidth utilization as the bandwidth is divided into several independent subbands for four LEDs and it needs some number of subcarriers as guard bands to avoid OOBI. From Fig. 9 (b), the results rerify that the proposed adaptive transmission scheme efficiently satisfies the QoS requirements of devices.

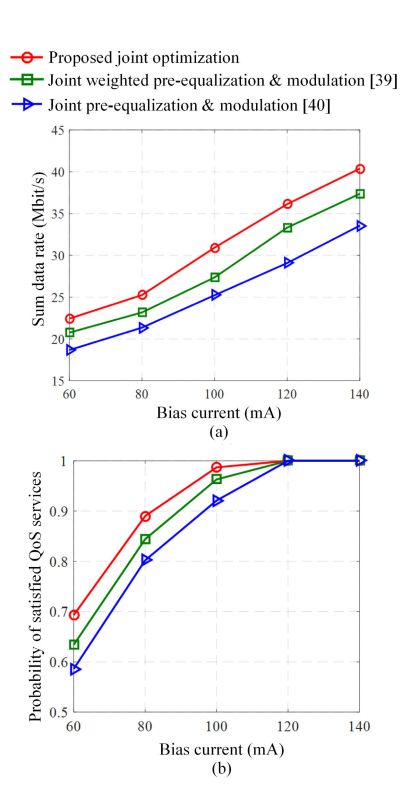


Fig. 9. (a) Sum transmission data rate and (b) the QoS satisfaction level under different bias currents (mA).

#### G. Localization Performance Under Different Scenarios

Here, we provide simulations to evaluate the effect of the reflected paths on the localization performance of our proposed system over the  $3 \times 3$  m<sup>2</sup> coverage area, and we also compare the localization performance between DPDOA and PDOA. As shown in Fig.10 (a), for DPDOA with reflected paths, the localization errors are mainly ranging from 3 to 8 cm, and some localization errors are more than 10 cm when the device is at corner or edge of the coverage area, and the mean positioning error is as high as 5.73 cm. From Fig. 10 (b), we can observe that for the DPDOA without reflected paths, most of the localization errors are less than 3 cm and only a few of them are more than 10 cm when the device is at edge or corner, and the mean positioning error is 3.47 cm. These results indicate that the localization accuracy will decrease due to the negative effect of the reflected paths. However, for PDOA, the positioning errors are mainly ranging from 5 to 10 cm, and the localization error is higher than 20 cm when the device locates near the room edge, and the mean positioning error is as high as 8.04 cm. Compared with PDOA, DPDOA does not need the help of LOs, and thus can avoid the negative effect on LOs of both system set up and localization accuracy.

#### H. The Effect of Power Allocation Values on Performance

Here, we provide related results to demonstrate the trade-off between communication and positioning. Here, let  $P_{\rm tot}$  denotes the total transmission power and  $\alpha$  denote the power allocation trade-off value between communication and positioning, where the allocated power for communication is

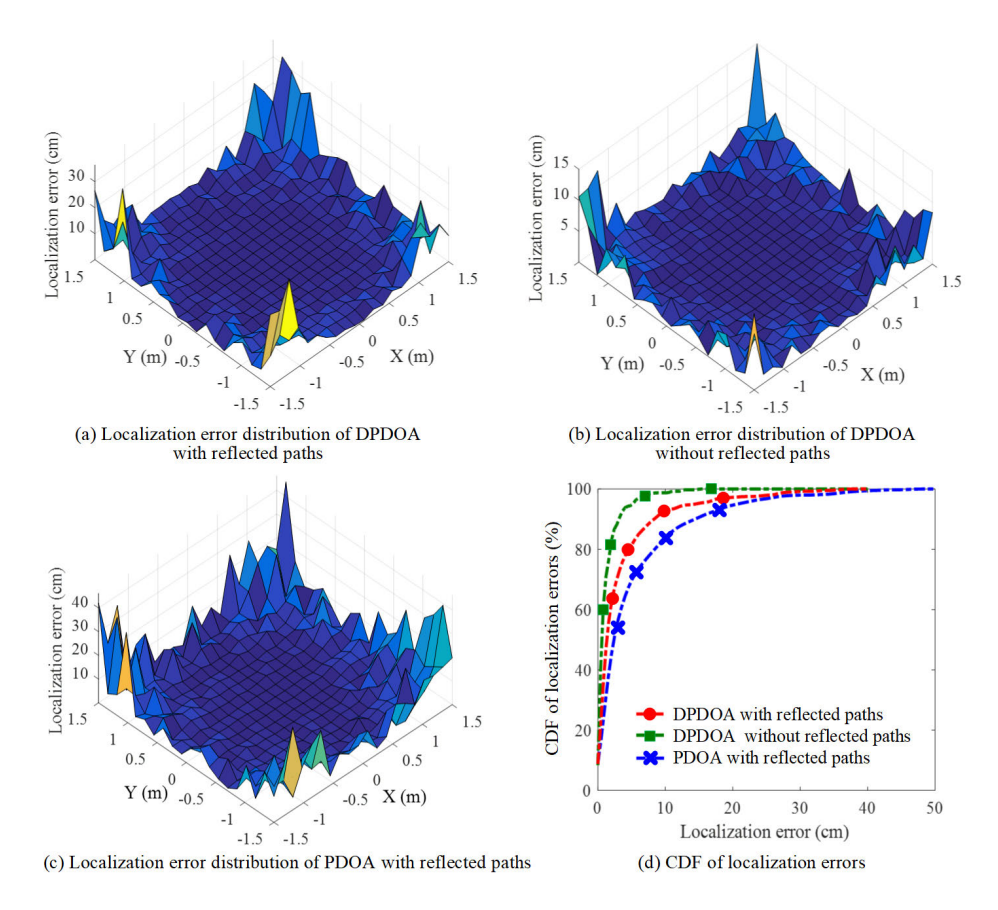


Fig. 10. Localization error distribution analysis under different scenarios.

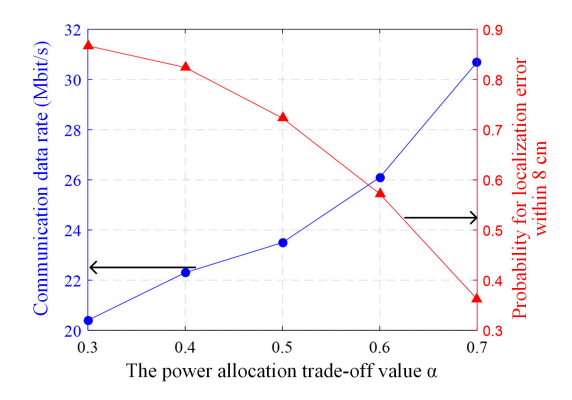


Fig. 11. The impact of the power allocation trade-off value on communication and localization performances.

 $P_{\mathrm{com}} = \alpha P_{\mathrm{tot}}$  and the allocated power for positioning is  $P_{\mathrm{pos}} = (1 - \alpha) P_{\mathrm{tot}}$ . In this context,  $P_{\mathrm{tot}} = P_{\mathrm{com}} + P_{\mathrm{pos}}$ .

Fig. 11 illustrates the effect of the power allocation trade-off value on the integrated VLCL system with the communication and positioning performances when the total bias current is 140 mA and the localization error threshold is 8 cm. Note that the transmit power is determined by the bias current at transmitters. When the trade-off value  $\alpha$  is 0.4, the probability for localization errors within 8 cm is 82.4% and the achievable data rate is 22.3 Mbps. From Fig. 11, we also can observe that as the increase of  $\alpha$ , the more power will be allocated for communication and thus the data rate enhances during this process. However, as the power allocated for positioning

decreases, the positioning error increases (positioning accuracy reduces) accordingly. It is worth noting that when the trade-off value  $\alpha$  changes from 0.6 to 0.7, the probability for localization errors within 8 cm significantly decreases from 57.2% to 36.3%. This phenomenon indicates that the positioning error is super big when the power allocated for positioning is less than  $0.4*P_{\rm tot}$ . In addition, we also find that the communication data rate decreases when  $\alpha$  changes from 0.4 to 0.3.

## V. CONCLUSION

This paper has proposed a realistic integrated VLCL system that can be used to support indoor real-time tracking and communication services. We implemented and experimented both tracking and communication operations on mobile devices in a real indoor environment. As RSS-based localization is much sensitive to random tilting of PD plane and background noise, an A-DPDOA-based localization algorithm is presented to provide high-accuracy localization. The experimental results illustrated that the presented system and robust schemes improve localization accuracy compared with existing solutions. Our future work will focus on the application the integrated VLCL system in 6G communications and industrial indoor environments [41].

#### REFERENCES

 H. Yang, A. Alphones, W.-D. Zhong, C. Chen, P. Du, and S. Zhang, "QoS-driven optimized design in a new integrated visible light communication and positioning system," in *Proc. IEEE Int. Conf. Commun.* (ICC), Jun. 2020, pp. 1–6.

- [2] C. Laoudias, A. Moreira, S. Kim, S. Lee, L. Wirola, and C. Fischione, "A survey of enabling technologies for network localization, tracking, and navigation," *IEEE Commun. Surveys Tuts.*, vol. 20, no. 4, pp. 3607–3644, 4th Quart., 2018.
- [3] H. Yang, W.-D. Zhong, C. Chen, and A. Alphones, "Integration of visible light communication and positioning within 5G networks for Internet of Things," *IEEE Netw.*, vol. 34, no. 5, pp. 134–140, Sep. 2020.
- [4] M. F. Keskin, A. D. Sezer, and S. Gezici, "Localization via visible light systems," *Proc. IEEE*, vol. 106, no. 6, pp. 1063–1088, Jun. 2018.
- [5] A. Jovicic, J. Li, and T. Richardson, "Visible light communication: Opportunities, challenges and the path to market," *IEEE Commun. Mag.*, vol. 51, no. 12, pp. 26–32, Dec. 2013.
- [6] H. Haas, L. Yin, Y. Wang, and C. Chen, "What is LiFi?" J. Lightw. Technol., vol. 34, no. 6, pp. 1533–1544, Mar. 15, 2016.
- [7] Z. Wang, Z. Yang, Q. Huang, L. Yang, and Q. Zhang, "ALS-P: Light weight visible light positioning via ambient light sensor," in *Proc. IEEE Conf. Comput. Commun. (INFOCOM)*, Apr. 2019, pp. 1306–1314.
- [8] S. R. Teli, P. Chvojka, S. Vítek, S. Zvanovec, R. Perez-Jimenez, and Z. Ghassemlooy, "A SIMO hybrid visible-light communication system for optical IoT," *IEEE Internet Things J.*, vol. 9, no. 5, pp. 3548–3558, Mar. 2022.
- [9] T. Komine and M. Nakagawa, "Fundamental analysis for visible-light communication system using LED lights," *IEEE Trans. Consum. Elec*tron., vol. 50, no. 1, pp. 100–107, Feb. 2004.
- [10] Y. Yang, J. Luo, C. Chen, Z. Chen, W.-D. Zhong, and L. Chen, "Pushing the data rate of practical VLC via combinatorial light emission," *IEEE Trans. Mobile Comput.*, vol. 20, no. 5, pp. 1979–1992, May 2021.
- [11] H. Chen, A. T. L. Lee, S.-C. Tan, and S. Y. Hui, "Electrical and thermal effects of light-emitting diodes on signal-to-noise ratio in visible light communication," *IEEE Trans. Ind. Electron.*, vol. 66, no. 4, pp. 2785–2794, Apr. 2019.
- [12] K. N. Datta et al., "Exploring visible light communication system using RTS/CTS mechanism for mobile environment, in *Proc. 24th Annu. Int. Conf. Mobile Comput. Netw.*, 2019, pp. 732–734.
- [13] C. Chen, S. Fu, X. Jian, M. Liu, X. Deng, and Z. Ding, "NOMA for energy-efficient LiFi-enabled bidirectional IoT communication," *IEEE Trans. Commun.*, vol. 69, no. 3, pp. 1693–1706, Mar. 2021.
- [14] S. Zhao, J. Xu, and O. Trescases, "Burst-mode resonant LLC converter for an LED luminaire with integrated visible light communication for smart buildings," *IEEE Trans. Power Electron.*, vol. 29, no. 8, pp. 4392–4402, Aug. 2014.
- [15] S. Niu, P. Wang, S. Chi, Z. Liu, W. Pang, and L. Guo, "Enhanced optical OFDM/OQAM for visible light communication systems," *IEEE Wireless Commun. Lett.*, vol. 10, no. 3, pp. 614–618, Mar. 2021.
- [16] R. Bai, Z. Wang, R. Jiang, and J. Cheng, "Interleaved DFT-spread layered/enhanced ACO-OFDM for intensity-modulated direct-detection systems," *J. Lightw. Technol.*, vol. 36, no. 20, pp. 4713–4722, Oct. 15, 2018.
- [17] S. D. Dissanayake and J. Armstrong, "Comparison of ACO-OFDM, DCO-OFDM and ADO-OFDM in IM/DD systems," *J. Lightw. Technol.*, vol. 31, no. 7, pp. 1063–1072, Apr. 1, 2013.
- [18] X. Huang, F. Yang, C. Pan, and J. Song, "Pre-distorted enhanced ADO-OFDM for hybrid VLC networks: A mutual-interference-free approach," *IEEE Photon. J.*, vol. 12, no. 2, pp. 1–12, Apr. 2020.
- [19] J. He, J. He, and J. Shi, "An enhanced adaptive scheme with pairwise coding for OFDM-VLC system," *IEEE Photon. Technol. Lett.*, vol. 30, no. 13, pp. 1254–1257, Jul. 1, 2018.
- [20] Y. Hong et al., "Experimental investigation of multi-band OCT precoding for OFDM-based visible light communications," *Opt. Exp.*, vol. 25, no. 11, pp. 12908–12914, May 2017.
- [21] K. Qiu, F. Zhang, and M. Liu, "Let the light guide us: VLC-based localization," *IEEE Robot. Autom. Mag.*, vol. 23, no. 4, pp. 174–183, Dec. 2016.
- [22] H.-S. Kim, D.-H. Kwon, S.-H. Yang, Y.-H. Son, and S.-K. Han, "Channel assignment technique for RF frequency reuse in CA-VLC-based accurate optical indoor localization," *J. Lightw. Technol.*, vol. 32, no. 14, pp. 2544–2555, Jul. 15, 2014.
- [23] S. Shao, A. Khreishah, and I. Khalil, "Enabling real-time indoor tracking of IoT devices through visible light retroreflection," *IEEE Trans. Mobile Comput.*, vol. 19, no. 4, pp. 836–851, Apr. 2020.
- [24] A. H. A. Bakar, T. Glass, H. Y. Tee, F. Alam, and M. Legg, "Accurate visible light positioning using multiple-photodiode receiver and machine learning," *IEEE Trans. Instrum. Meas.*, vol. 70, pp. 1–12, 2021.

- [25] C. Amini, P. Azmi, and S. S. Kashef, "An accurate ranging algorithm based on received signal strength in visible light communication," *J. Lightw. Technol.*, vol. 39, no. 14, pp. 4654–4660, Jul. 15, 2021.
- [26] H. Steendam, "A 3-D positioning algorithm for AOA-based VLP with an aperture-based receiver," *IEEE J. Sel. Areas Commun.*, vol. 36, no. 1, pp. 23–33, Jan. 2018.
- [27] C.-Y. Hong et al., "Angle-of-arrival (AOA) visible light positioning (VLP) system using solar cells with third-order regression and ridge regression algorithms," *IEEE Photon. J.*, vol. 12, no. 3, pp. 1–5, Jun. 2020.
- [28] L. Li, P. Xie, and J. Wang, "Enabling 3D ambient light positioning with mobile phones and battery-free chips," *IEEE Trans. Mobile Comput.*, vol. 20, no. 3, pp. 952–964, Mar. 2021.
- [29] S. M. Sheikh, H. M. Asif, K. Raahemifar, and F. Al-Turjman, "Time difference of arrival based indoor positioning system using visible light communication," *IEEE Access*, vol. 9, pp. 52113–52124, 2021.
- [30] S. Zhang, W.-D. Zhong, P. Du, and C. Chen, "Experimental demonstration of indoor sub-decimeter accuracy VLP system using differential PDOA," *IEEE Photon. Technol. Lett.*, vol. 30, no. 19, pp. 1703–1706, Oct. 1, 2018.
- [31] S. Zhang, P. Du, C. Chen, W.-D. Zhong, and A. Alphones, "Robust 3D indoor VLP system based on ANN using hybrid RSS/PDOA," *IEEE Access*, vol. 7, pp. 47769–47780, 2019.
- [32] 5GPPP Association. (Oct. 2015). 5G and the Factories of the Future, White Paper. [Online]. Available: https://5g-ppp.eu/wpcontent/uploads/2014/02/5G-PPP-White-Paper-on-Factories-of-the-Future-Vertical-Sector.pdf
- [33] B. Lin, X. Tang, Z. Ghassemlooy, C. Lin, and Y. Li, "Experimental demonstration of an indoor VLC positioning system based on OFDMA," *IEEE Photon. J.*, vol. 9, no. 2, pp. 1–9, Apr. 2017.
- [34] H. Yang, C. Chen, W.-D. Zhong, A. Alphones, S. Zhang, and P. Du, "Demonstration of a quasi-gapless integrated visible light communication and positioning system," *IEEE Photon. Technol. Lett.*, vol. 30, no. 23, pp. 2001–2004, Dec. 1, 2018.
- [35] H. Yang et al., "Coordinated resource allocation-based integrated visible light communication and positioning systems for indoor IoT," *IEEE Trans. Wireless Commun.*, vol. 19, no. 7, pp. 4671–4684, Jul. 2020.
- [36] H. Yang, W.-D. Zhong, C. Chen, A. Alphones, and P. Du, "QoS-driven optimized design-based integrated visible light communication and positioning for indoor IoT networks," *IEEE Internet Things J.*, vol. 7, no. 1, pp. 269–283, Jan. 2020.
- [37] D. Kim, J. K. Park, and J. T. Kim, "Three-dimensional VLC positioning system model and method considering receiver tilt," *IEEE Access*, vol. 7, pp. 132205–132216, 2019.
- [38] T. Yuan, Y. Xu, Y. Wang, P. Han, and J. Chen, "A tilt receiver correction method for visible light positioning using machine learning method," *IEEE Photon. J.*, vol. 10, no. 6, pp. 1–12, Dec. 2018.
- [39] Y. Wang, L. Tao, Y. Wang, and N. Chi, "High speed WDM VLC system based on multi-band CAP64 with weighted pre-equalization and modified CMMA based post-equalization," *IEEE Commun. Lett.*, vol. 18, no. 10, pp. 1719–1722, Oct. 2014.
- [40] Y. Xu et al., "Accuracy analysis and improvement of visible light positioning based on VLC system using orthogonal frequency division multiple access," Opt. Exp., vol. 26, no. 7, pp. 9230–9242, Apr. 2018.
- [41] H. L. Yang, "Visible light communication systems supporting wireless data access and indoor positioning applications," Ph.D. thesis, School Elect. Electron. Eng., Nanyang Technol. Univ., Singapore, Mar. 2020.



Helin Yang (Senior Member, IEEE) received the B.S. and M.S. degrees from the School of Telecommunications and Information Engineering, Chongqing University of Posts and Telecommunications, in 2013 and 2016, respectively, and the Ph.D. degree from the School of Electrical and Electronic Engineering, Nanyang Technological University, Singapore, in 2020. He is currently an Associate Professor with the School of Informatics, Xiamen University, Xiamen, China. His research interests include wireless communication and resource management.



Sheng Zhang received the B.E. degree from the School of Optical and Electric Information, Huazhong University of Science and Technology, in 2015, and the Ph.D. degree from the School of Electrical and Electronic Engineering, Nanyang Technological University, Singapore, in 2020. He is currently an Scientist with the Institute for Infocomm Research (I2R), A\*STAR, Singapore. His current research interests include air traffic systems, positioning systems, machine learning, and signal processing.



Arokiaswami Alphones (Senior Member, IEEE) received the B.Tech. degree from the Madras Institute of Technology, Chennai, India, in 1982, the M.Tech. degree from the Indian Institute of Technology Kharagpur, Kharagpur, India, in 1984, and the Ph.D. degree in optically controlled millimeter wave circuits from the Kyoto Institute of Technology, Kyoto, Japan, in 1992. Since 2001, he has been with the School of Electrical and Electronic Engineering, Nanyang Technological University, Singapore. His current research interests include electromagnetic

analysis on planar RF circuits and integrated optics, microwave photonics, and wireless power transfer technologies.



Chen Chen (Member, IEEE) received the B.S. and M.Eng. degrees from the University of Electronic Science and Technology of China, Chengdu, China, in 2010 and 2013, respectively, and the Ph.D. degree from Nanyang Technological University, Singapore, in 2017. He was a Post-Doctoral Researcher with the School of Electrical and Electronic Engineering, Nanyang Technological University, from 2017 to 2019. He is currently a Research Professor with the School of Microelectronics and Communication Engineering, Chongqing University,

Chongqing, China. His research interests include optical wireless communication, optical access networks, the Internet of Things, and machine learning.



Kwok-Yan Lam (Senior Member, IEEE) received the B.Sc. degree (Hons.) from the University of London in 1987 and the Ph.D. degree from the University of Cambridge in 1990. He was a Visiting Scientist with the Isaac Newton Institute, University of Cambridge; and a Visiting Professor with the European Institute for Systems Security. He has collaborated extensively with law-enforcement agencies, government regulators, telecommunication operators, and financial institutions in various aspects of infocomm and cyber security in the region. He was

a Professor with Tsinghua University, China, from 2002 to 2010. He has been a Faculty Member of the National University of Singapore and the University of London, since 1990. He is currently a renowned cyber security researcher and a practitioner. He is also a Full Professor with Nanyang Technological University. In 1998, he received the Singapore Foundation Award from the Japanese Chamber of Commerce and Industry, in recognition of his research and development achievement in information security in Singapore.



Zehui Xiong (Senior Member, IEEE) received the Ph.D. degree from Nanyang Technological University (NTU), Singapore. He is currently an Assistant Professor with the Singapore University of Technology and Design, and also an Honorary Adjunct Senior Research Scientist with Alibaba–NTU Singapore Joint Research Institute, Singapore. He was the Visiting Scholar with Princeton University and the University of Waterloo. He has published more than 200 research papers in leading journals and flagship conferences and many

of them are ESI highly cited papers. His research interests include wireless communications, the Internet of Things, blockchain, edge intelligence, and metaverse. He has won over ten best paper awards in international conferences and is listed in the World's Top 2% Scientists identified by Stanford University. He was a recipient of the IEEE Early Career Researcher Award for Excellence in Scalable Computing, the IEEE Technical Committee on Blockchain and Distributed Ledger Technologies Early Career Award, the IEEE Internet Technical Committee Early Achievement Award, the IEEE TCSVC Rising Star Award, the IEEE TRANSACTIONS ON COMPUTATIONAL IMAGING Rising Star Award, the IEEE TCCLD Rising Star Award, the IEEE Best Land Transportation Paper Award, the IEEE CSIM Technical Committee Best Journal Paper Award, the IEEE SPCC Technical Committee Best Paper Award, the IEEE VTS Singapore Best Paper Award, the Chinese Government Award for Outstanding Students Abroad, and the NTU SCSE Best PhD Thesis Runner-Up Award. He is serving as the Associate Director for the Future Communications Research and Development Program. In 2023, he was featured on the list of Forbes Asia 30 under 30. He is serving as an Editor or the Guest Editor for many leading journals, including IEEE JOURNAL ON SELECTED AREAS IN COMMUNICATIONS, IEEE TRANSACTIONS ON VEHICULAR TECHNOLOGY, IEEE INTERNET OF THINGS JOURNAL, IEEE TRANSACTIONS ON COGNITIVE COMMUNICATIONS AND NETWORKING. and IEEE Transactions on Network Science and Engineering.



Liang Xiao (Senior Member, IEEE) received the B.S. degree in communication engineering from the Nanjing University of Posts and Telecommunications, China, in 2000, the M.S. degree in electrical engineering from Tsinghua University, China, in 2003, and the Ph.D. degree in electrical engineering from Rutgers University, NJ, USA, in 2009. She was a Visiting Professor with Princeton University, Virginia Tech, and the University of Maryland, College Park. She is currently a Professor with the Department of Information and Communication

Engineering, Xiamen University, Xiamen, China. She was a recipient of the Best Paper Award for 2016 INFOCOM Big Security WS and the 2017 ICC. She has served as an Associate Editor for IEEE TRANSACTIONS ON INFORMATION FORENSICS AND SECURITY and the Guest Editor for IEEE JOURNAL OF SELECTED TOPICS IN SIGNAL PROCESSING.



Yi Zhang (Member, IEEE) received the B.S. degree in software engineering from Xiamen University in 2014 and the M.S. and Ph.D. degrees in communication engineering from the National Taiwan University, in 2016 and 2020, respectively. He was with the Quanzhou Institute of Equipment Manufacturing, Chinese Academy of Sciences, from 2016 to 2017. He is currently an Assistant Professor with the Department of Information and Communication Engineering, Xiamen University. His research interests include mobile and wire-

less networking, fog/edge computing, and game theoretical models for communications networks.